Stark-Zeeman line shape model for multi-electron radiators in hot and dense plasmas submitted to large magnetic fields

Sandrine Ferri, Olivier Peyrusse, Annette Calisti

Stark-Zeeman line shape model for multi-electron radiators in hot and dense plasmas submitted to large magnetic fields.

Sandrine Ferri,[1] Olivier Peyrusse,[1] and Annette Calisti[1]

Aix-Marseille Univ., CNRS, PIIM, UMR7345, Marseille, France.

(*Electronic mail: corresponding author: sandrine.ferri@univ-amu.fr)

(Dated: 15 September 2021)

We present a Stark-Zeeman spectral line shape model and the associated numerical code, PPPB, designed to provide fast and accurate line shapes for arbitrary atomic systems for a large range of plasma conditions. PPPB is based on the coupling of the PPP code, a Stark broadened spectral line shape code, developed for multi-electron ion spectroscopy in hot and dense plasmas, and the MASCB code, recently developed to generate B-field dependent atomic physics. The latter provides energy levels, statistical weights and reduced matrix elements of multi-electron radiators by diagonalizing the atomic Hamiltonian which includes the well know B-dependent term. They are used as input in PPP working in the standard line broadening approach, i.e. using the quasi-static ion and impact electron approximations. The ion dynamics effects are introduced by the mean of the frequency fluctuation model (FFM). The physical model of the electron broadening is based on the semi- classical impact approximation including the effects of a strong collision term, of interference and cyclotron motion. Finally, to account for polarization effects, the output profiles are calculated for a given angle of observation with respect to the direction of the magnetic field. The potential of such model is presented through Stark-Zeeman spectral line shape calculations performed for various experimental conditions.

PACS numbers: Spectral line shapes modeling, Plasmas, Magnetic fields

I. INTRODUCTION

Measurements of magnetic fields are of importance in many studies of laboratory or space plasmas. Among other methods, spectroscopic measurements are often used in plasmas to infer temperatures from line intensity ratio and Doppler broadening, electron densities from the Stark broadening and magnetic field strengths from distinct line shape features. The spectroscopy diagnostic techniques are based on the comparison between the observed and the modeled spectra. Therefore, their reliable implementation requires accurate calculations of emission or absorption spectra, which imply the use of analytic methods and computer codes of different complexity and limit of applicability. Line shape modeling in plasmas has a long history[1] but the existence of intense magnetic fields in astrophysical objects (e.g. white dwarfs) and in various types of plasmas created in laboratory (e.g., the magnetic- and inertial-confinement fusion devices) revives the interest for atomic physics developments in such extreme conditions.

The presence of magnetic fields increases the complexity of line shape calculations in plasmas. A magnetic field has three essential effects on Stark-broadened spectral lines: - a partial polarization of the emitted light, - an additional splitting according to value of the magnetic quantum number, m, and - the bending of the colliding charged particle trajectories into a helical path around the magnetic lines of forces. These effects have been studied for several decades both theoretically and experimentally since the initial work of N. Hoe and colleagues[2]. Different methods have been developed or have been extended to magnetized plasmas, such as numerical simulations[3–6], or various theoretical models[7–16]. Most of them are based on simplifying assumptions depending on the relative importance of the Stark and Zeeman effects. A measure of this relative importance is given by the ratio τ between the two respective average energy shifts[2]. For example, for hydrogen, with the normal electric field strength $F_0 = e/r_e^2$ and $r_e = (\frac{3}{4\pi N_e})^{1/3}$, where e is the elementary charge and N_e is the electron density, expressed in cm^{-3}, τ is given by

$$\tau = 5.15 \times 10^{-11} n N_e^{2/3} / B, \tag{1}$$

with n the principal quantum number and B the magnetic field strength, expressed in tesla. The line profile coincides with the pure Stark profile if $\tau \gg 1$ and deviates progressively as τ decreases. When $\tau \sim 1$, profiles broadened by the combined Stark-Zeeman effect are an intricate function of N_e and B. Such cases are found for low$-n$ hydrogen line series emitted in Tokamak edge regions

where $N_e \sim 10^{14}\ cm^{-3}$, $T_e \sim 1\ eV$ and $B \sim$ few teslas, or in white dwarfs, where signature of intense magnetic fields (over few hundred teslas) is observed at higher densities ($N_e \sim 10^{17}\ cm^{-3}$). In laser-produced plasmas ($100\ eV < T_e < 1\ keV$ and $10^{21} < N_e < 10^{24}\ cm^{-3}$), high magnetic fields over few hundreds teslas are generated and can strongly affect the emission of highly ionized atoms[17,18]. These conditions require a simultaneous treatment of Stark and Zeeman effects on the line broadening.

The goal of this work is to present the main feature of the Stark-Zeeman line shape code PPPB through various applications related to strongly magnetized plasmas.

II. ATOMIC PHYSICS IN PRESENCE OF MAGNETIC FIELDS

Atomic data necessary for a Stark-Zeeman calculation are usually generated by atomic physics codes free of any external field. In practice, we use the Cowan Hartree-Fock atomic structure code[19], the Multi Configuration Dirac Fock code (MCDF)[20], the Flexible Atomic Code (cFAC)[21,22] or homemade codes for neutrals. In its original form, PPPB was designed to solve the problem within the strong or the weak magnetic field approximations. The energy levels, statistical weights and reduced dipole matrix elements were externally generated and neglecting the quadratic contribution, the Zeeman contribution to the Hamiltonian was introduced in PPPB.

The Zeeman Hamiltonian reads

$$H_Z = \mu_B B(L_z + g_s S_z), \tag{2}$$

where B is the magnitude of the magnetic field along the z direction, μ_B is the Bohr magneton, $g_s = 2.0023192$ is the anomalous gyromagnetic ratio for the electron spin, and L_z and S_z, the projections of the total orbital and spin angular momenta of the atom, respectively. For sufficiently weak B-field values, the off-diagonal matrix elements of H_Z that connect states of different values of the modulus, J, of the total angular momentum of the system, $\vec{J} = \vec{L} + \vec{S}$, are negligible compared to the contributions of the Coulomb and spin-orbit interactions. The contribution of the magnetic field to the energy can be calculated as a perturbation. The following expression of the diagonal matrix element of H_Z for the state $|\gamma\ J\ M\rangle$ was retained in PPPB

$$\langle \gamma\ J\ M| \left(L_z + g_s S_z\right) |\gamma\ J\ M\rangle = g_{\gamma J} M, \tag{3}$$

where $g_{\gamma J}$ is the Landé factor of the level $\gamma\, J$[19]. For magnetic fields sufficiently strong to disrupt the coupling between orbital $\vec{L}$ and spin $\vec{S}$ momenta, L_z and S_z are easily evaluated for a state $|\gamma\, L\, S\, m_l\, m_s\rangle$. The strong field approximation through the following expression was then retained

$$\langle \gamma\, L\, S\, m_l\, m_s | \left(L_z + g_s S_z\right) | \gamma\, L\, S\, m_l\, m_s \rangle = m_l + g_s m_s. \tag{4}$$

One can consider that the weak- and strong-field approaches are no longer valid when the magnetic field and the spin-orbit contributions are of the same order of magnitude. In this intermediate case, the diagonalization of the whole Hamiltonian $\xi \vec{L}\cdot\vec{S} + \mu_B \vec{B}(\vec{L} + g_s\vec{S})$ is necessary.

An estimate of the critical B-field values, B_c (in tesla), for which both contributions have to be considered at the same level in the Hamiltonian, is given for one-electron configuration[23]

$$B_c \sim \left(\frac{Z^*}{n}\right)^4 \left(\frac{e^2}{\hbar c}\right)^2 \frac{m_e e^4}{\mu_B \hbar^2}, \tag{5}$$

with Z^* the effective charge, given by the Slater's rule: $Z^* = Z - \sigma$, where σ is the screening constant[24].

Table I shows the values of B_c for some H-like ($Z^* = Z$) and Li-like ($Z^* = Z - 2\sigma_{1s}$, with $\sigma_{1s} = 0.85$) ions of interest. Radiative transitions from $n = 2$ are assumed.

Element	$B_c(tesla)$	
	H-like	Li-like
H (Z=1)	0.78	$--$
C (Z=6)	10^3	270
Si (Z=14)	30×10^3	18×10^3
Ar (Z=18)	80×10^3	55×10^3

TABLE I. Critical value of the magnetic field (in tesla) for which the spin-orbit interaction is of the same order of magnitude as the magnetic interaction. Estimations are made for Hydrogen-like and Lithium-like ionization stages for elements of interest in this work.

To go beyond the weak and strong field approximations mentioned above, the atomic physics

code MASCB has been developed to generate B-field dependent atomic physics quantities.

MASCB follows the usual approach where the N-electron atomic Hamiltonian H is divided into two parts. A separable part where electrons are supposed to be independent in a central potential. The corrective part is treated using perturbation theory. In this framework, multi-electron atomic states appear formally as a combination of Slater determinants. This means that, matrix elements of H, J^2 and J_z must be calculated and the eigenvectors of these operators obtained after diagonalization are the eigenstates of the atomic system. After an identification of the useful (i.e. restricted, see for instance[25,26]) Slater determinant belonging to a set of configurations, matrix elements are calculated using Condon rules summarized in classical textbooks[24,27]. The restriction of the Slater determinant set consists in considering just one possible value of M (eigenvalue of J_z) which is common to all states of a set of configurations. The subsequent calculations of transition matrix elements coupling states of different M make use of the Wigner-Eckart theorem and of operators J_+ or J_- when needed. After a sequential treatment of a list of configuration, it is still possible to diagonalize the atomic Hamiltonian in the basis of the states belonging to all of the considered configurations, which is just the so-called superposition of configurations method.

The description is non-relativistic, i.e. based on the Schrödinger equation, but it incorporates the main relativistic corrections to the central field potential[19]. This central potential, from which mono-electronic energies and orbitals are obtained self-consistently, is built in the framework of the Optimized Effective Potential method[28,29].

After the primary treatment of the *isolated* atom, one diagonalizes the part of the Hamiltonian describing the interaction with the magnetic field. This part reads (in SI units)

$$H_B = H_Z + \frac{e^2B^2}{8m_e}\sum_i^N r_i^2 sin^2\theta_i, \tag{6}$$

where H_Z is the linear Zeeman term (Eq.2), the second term being the quadratic term. Here r_i, θ_i are the usual polar coordinates of electron i in a system where the polar axis is taken along the B axis, i.e. the z-axis[30].

It is worth noting that the quadratic term of H_B introduces a mixing between states of different n making the matrix of infinite order. Here the eigenvalues are necessarily approximated by those

of a truncated Hamiltonian matrix for H_B. Truncated because this matrix is limited to a preselected set of configurations. For a given value of the magnetic field, it is then necessary to check whether the addition of more configurations introduces a significant change on the eigenvalues of interest. For hydrogen or helium atoms this method has proven to yield sufficiently accurate results[30]. The figure 1 shows the effect of the quadratic terms on the Balmer series lines of hydrogen (up to $H-\varepsilon$ that corresponds to the radiative transition from $n=7$ to $n=2$)[31,32] for plasma conditions relevant to white dwarf atmospheres[33]. One compares the Stark-Zeeman profiles obtained accounting or not for the quadratic B-field effects for three magnetic field values: a) $B=100$ $tesla$, b) $B=500$ $tesla$ and c) $B=1$ $ktesla$. The calculations have been performed over the entire Balmer series at once. Stark coupling between upper levels with different principal quantum numbers have been accounted for. Note that our atomic structure calculation is performed in a configuration interaction mode where the mixing is introduced by the quadratic term. This last point is crucial for proper consideration of this term.

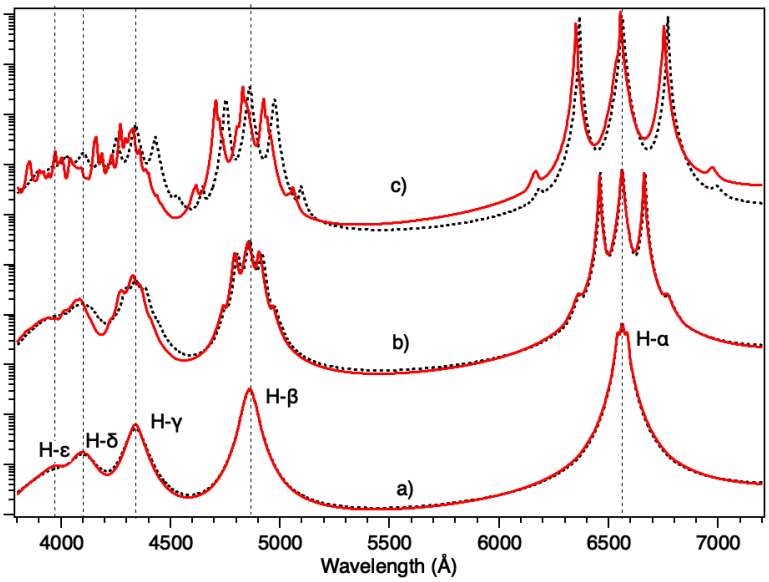

FIG. 1. Stark-Zeeman broadened Balmer series lines for $N_e \sim 10^{17}$ cm^{-3}, $k_BT=5$ eV and a) $B=100$ $tesla$, b) $B=500$ $tesla$ and c) $B=1$ $ktesla$, without quadratic terms (dash) and with quadratic terms (solid). The direction of observation is transversal to the B-field direction.

The quadratic terms give rise to additional structures on the line shapes and to a global shift that increases as the principal quantum number increases. For higher magnetic fields, the Zeeman components from different principal quantum numbers merge, so that the line series resemble as complex set of indiscernible lines. Inferring the B-field from those lines is no longer possible.

In addition, the measure of the electron density by the mean of the Inglis-Teller limit[34] can lead to an overestimation of the electron density if Zeeman effects are not considered in the calculation. As for example, the largest principal quantum number (PQN) given by the Inglis-Teller limit is nearly equal to 7 for an electron density equal to $10^{17}\ cm^{-3}$. The Stark-Zeeman Balmer series verify this limit for a magnetic field of the order of 100 tesla. But, the lines emitted from large quantum numbers start to merge as the B-field increases. For $B = 500\ tesla$, the last resolved lines correspond to the H_δ transitions, i.e. from the upper level $n = 6$. Using this level as the largest PQN to infer the electron density would give $N_e \sim 2.7 \times 10^{17}\ cm^{-3}$ instead of $N_e = 10^{17}\ cm^{-3}$ as the calculation was performed. For $B = 1\ ktesla$, the last resolved lines correspond to the H_γ transitions, i.e. from the upper level $n = 5$. Hence the corresponding inferred electron density would be $N_e = 10^{18} cm^{-3}$, an order of magnitude higher than the right one.

III. HELICAL TRAJECTORIES

Another difficulty to overcome in magnetized plasmas, is that, the charged particles follow helical trajectories. The gyromotion of the electrons and ions around the magnetic lines of forces may alter the dynamics of the plasma particles. Recent studies in strongly coupled magnetized plasmas, i.e., when the Coulomb interaction exceeds the kinetic energy of the particles, have reported a strong influence of the helical trajectories on the transport properties[35–37]. A significantly curved trajectory will also change the emitter-perturber interaction dynamics. Of particular current interest are the electric microfield statistical properties in the case of strongly magnetized plasmas. The Stark-Zeeman broadening mechanisms of spectral line shape could then be affected.

The effect of the helical trajectory on the emitter-perturber interaction can be estimated by the ratio of the Debye length $\lambda_D = \sqrt{\frac{k_B T}{4\pi N_e e}}$ to the Larmor radius $r_L = \sqrt{k_B T mc^2}/ZeB$, with m, T and Z the particle mass, temperature and charge, respectively. When the Larmor radius remains the same order of the Debye length, the pertuber gyration occurs on the same time and length scales as the Coulomb interaction. Above a critical B-field B_h, that corresponds to $\lambda_D/r_L = 1$, the helical trajectory has then to be accounted for. As illustration, values of the critical B-field for electrons in magnetized plasmas of interest are summarized in Table II.

Magnetized plasmas	$N_e\ (cm^{-3})$	$B_h(tesla)$
Tokamak edge plasmas ($B \sim$ a few $tesla$)	10^{13}	1
White Dwarf ($B \sim 100\ T - 1\ ktesla$)	10^{17}	100
Laser plasmas ($B < 500\ T$)	10^{20}	3.2×10^3
Imploded targets ($B \sim$ a few $ktesla$)	10^{23}	100×10^3

TABLE II. Columns list plasma of interest (with the magnetic field values commonly measured in the concerned plasmas), electron density (N_e) and critical B-field B_h for electrons.

Recent studies of the influence of B-fields on the electron trajectories in hydrogen plasmas have been performed in the context of magnetic fusion and white dwarfs[38–41]. It has been shown that the introduction of helical trajectories reduces the characteristic duration of the perturbation to the order of the inverse of the Larmor frequency, $\tau_L = 2\pi/\omega_L = 2\pi m_e c/eB$. This results in a line shape narrowing. Such results suggest a modification of the electron collision operator generally used to describe the electronic Stark effect in line shape modeling, as we will see in section IV C.

Concerning the effects of helical trajectories on the interaction between the radiator and the ionic perturbers, investigations of the statistical properties of the ionic microfields using classical Molecular Dynamics simulations have been performed for short-pulse laser experiment conditions where magnetic fields of a few thousands of tesla have been measured[3]. It has been shown that the modification of ionic field distribution function, $W(F)$, by the magnetic field was negligible. The same conclusion was exposed by C. Deutsch[42]: *"The low frequency component of the electric microfields is seen to be rigorously unaffected by magnetic field in a thermal plasma"*, but, to conclude: *"in presence of a very strong magnetic field [ ] the slow electrons are to be added to the ionic part of the low frequency component."*. Very recent MD simulations[43], in the context of high B-field generation using laser-plasmas interactions[17] have shown that the helical trajectories of the electrons along the B-line of forces may affect the distribution of the electrons around the ions and thus may indirectly affect the ionic microfield distribution functions. Such results are preliminary and more investigations have to be done.

IV. PPPB : A STARK-ZEEMAN LINE SHAPE CODE

The spectral line shape code PPPB has been designed to provide Stark-Zeeman broadened line shapes for a wide range of density, temperature, and magnetic field values[14]. It is based on the PPP code, a Stark-broadened spectral line shape code[44,45], developed some years ago for multi-electron ion spectroscopy in inertial confinement fusion plasmas[46,47].

Line shapes are usually modeled by working in the "standard" quasi-static ion/impact electron limit. The line shape function is given by

$$I_s(\omega) = \int_0^\infty W(F_i) I(\omega, F_i) dF_i, \tag{7}$$

where, ω is the photon frequency and $I(\omega, F_i)$ is the electron broadened line profile for a given value of the microfield F_i following the static ion microfield distribution function, $W(F_i)$. The field-dependent profile reads

$$I(\omega, F_i) = \frac{1}{\pi} ReTr\Big\{ d^\dagger [i\omega - iL(F_i) + \phi(\omega)]^{-1} \rho d \Big\} \tag{8}$$

where $L(F_i) = [H_Z(F_i), I]$ is the Liouville operator associated to the B-field dependent Hamiltonian of the emitter H_Z, ρ is the emitter density operator, d is the emitter dipole operator and $\phi(\omega)$ is the electron broadening operator (see section IV C).

A peculiarity of Zeeman effect is a quantization axis imposed by the magnetic field. This implies the emission to be polarized, following the selection rules for the dipole radiation, $\Delta J = J' - J = 0, \pm 1$ ($J' = J = 0$ not allowed), $q = \Delta M = M' - M = \pm 1$ ($\sigma_\pm$ polarizations) and $q = \Delta M = 0$ (π polarizations), assuming the magnetic field in the direction z. As the symmetry is broken, the integration over the ionic microfield implies to consider the three directions of space separately. One defines $\vec{F}_\parallel$ and $\vec{F}_\perp$ the parallel and perpendicular ionic microfields to the direction of the magnetic field, respectively. If θ is the angle between the magnetic and the electric fields, then $F_\parallel = F_i \mu$ and $F_\perp = F_i \sqrt{1-\mu^2}$, with $\mu = \cos\theta$. Therefore, the line profile given by Eq.(7) is written as

$$I_{s,q}(\omega) = \frac{1}{2} \int_0^\infty W(F_i) \int_{-1}^{+1} I_q(\omega, F_i, \mu) d\mu dF_i, \tag{9}$$

where $I_q(\omega, F_i, \mu)$ represents the $q-$polarized line profile emitted by an ion in an external magnetic field and in a static ion field F_i.

The emission profile observed in the line of sight of the observer is given, by

$$I(\omega,\alpha) = I_{\parallel}(\omega)cos^2(\alpha) + I_{\perp}(\omega)sin^2(\alpha), \tag{10}$$

where α is the angle between the line of sight of the observer and the direction of $\vec{B}$ and

$$I_{\parallel}(\omega) = I_{+1}(\omega) + I_{-1}(\omega), \tag{11}$$

$$I_{\perp}(\omega) = I_0(\omega) + \frac{1}{2}(I_{+1}(\omega) + I_{-1}(\omega)), \tag{12}$$

where $I_{-1}(\omega)$, $I_0(\omega)$ and $I_{+1}(\omega)$ are the q-polarized components given in Eq (9), $q = -1, 0, +1$ respectively.

The calculation of the integrant in Eq.(9) involves the inversion and the product of matrices in the complex domain. In principle the calculation of has to be done for every static ion microfield point and for every frequency point in the line shape, $I_s(\omega)$. This is the most time-consuming task in a line shape code. Hence, computer power and efficient algorithms are essential to make complex emitter line shape calculations practical.

A. Static profile and Stark dressed transitions

The PPPB code performs block diagonalization of the resolvent in Eq.(8), afforded by the selection rules of the atomic matrix elements. It performs an eigen-decomposition of the resolvent in the $\{f,\mu\}$-dependent bases (see ref.[14,44,48] for more details)

$$I_{s,q}(\omega) = \sum_f W_f^{(2)} \sum_\mu W_\mu^{(G)}\, Im \ll d_q^\dagger | M_{f,\mu} \left[\omega 1 - L^d(f,\mu)\right]^{-1} M_{f,\mu}^{-1} | d_q \rho_0 \gg, \tag{13}$$

where $M_{f,\mu}$ is the matrix that diagonalizes the Liouville operator L: $M_{f,\mu}^{-1} L(f,\mu) M_{f,\mu} = L^d(f,\mu)$. The integration over F_i and μ are replaced by i) a two-point integration weight, used for the summation over the discrete ionic field intensities f, and, ii) a Gauss-Legendre quadrature weight, used for the angle summation[49]. The number of microfields necessary to well describe the static distribution function is $n_f \sim 50$ and a value of $n_\mu \sim 30$ is enough to have a good convergence in the angle summation.

In the PPPB code the static microfield distribution functions are either estimated from classical Molecular Dynamics (MD) simulations[50], or by the Adjustable Parameter EXponential (APEX) model[51,52]. The latter is computationally fast and suited for weakly as well as strongly coupled plasmas. Note to mention that, the Hooper static-field distribution function is used for the calculations involving neutral emitters[53]. Accordingly, all those models do not depend on B and consider the plasma surrounding the emitter isotrope.

This procedure leads to the concept of the Stark spectral components emitted by a set of dressed two-level radiators: the Stark-dressed transitions (SDT). The SDT are characterized by two complex numbers namely the generalized intensity $a_{q,k} + ic_{q,k}$ and the generalized frequency $f_{q,k} + i\gamma_{q,k}$.

The static q-polarized profile is then described by a sum of rational fractions which are generalized Lorentzian spectral components of the line,

$$I_{s,q}(\omega) = \sum_{k=1}^{n_{q,k}} \frac{c_k(\omega - f_{q,k}) + a_{q,k}\gamma_{q,k}}{(\omega - f_{q,k})^2 + \gamma_{q,k}^2} \tag{14}$$

with $n_{q,k} = n_f \times n_\mu \times n_e \times n_g$ the number of SDT, that is also proportional to n_g and n_e the number of ground and upper selected energy levels, respectively, that define the studied atomic system.

B. The Frequency Fluctuation Model: stochastic mixing of the SDT

The quasi-static approximation is a useful approximation. But it is well known that a quasistatic treatment of the ion perturbation can lead to large errors for plasma conditions that yield substantial microfield fluctuations[54]. Depending on the time scale of the line emission, the fluctuations of the microfields, produced by the moving ions, have to be accounted for. This is the most difficult part of the line broadening problem due to the stochastic behavior of the microfields[55].

The ion dynamics producing microfield fluctuations is modeled, in PPPB, by using the Frequency Fluctuation Model (FFM)[14,56].

The FFM is based on the assumption that an atomic system perturbed by a fluctuating microfield behaves like a set of SDTs that are subject to a stationary Markov mixing process induced by the field fluctuation. This results in an effective exchange between two-level transitions following a Poisson process with the fluctuation rate of $\nu_i = v_{th}/r_i$, with v_{th} the ion thermal velocity and $r_i = (\frac{4}{3}\pi N_i)^{-1/3}$ the mean distance between the ions, assuming a ionic density N_i.

Working in the Liouville space of the SDT, the Stark-Zeeman line shape accounting for the ion dynamics and polarization is written as

$$I_{d,q}(\omega) = Re\frac{1}{\pi}\sum_{kj} i\left\langle D_{d,k}\right| \Big(\omega 1 - L^d - i\Gamma + iW\Big)^{-1} \left|D_{q,j}\right\rangle p_{q,j}, \tag{15}$$

with L^d the Liouville operator involving the transition frequencies of the SDT, $D_{q,j} = r_q\sqrt{1+ic_j/a_j}$ the matrix elements of the dipole moement for the SDT in the q polarization state ($r_q^2 = \sum_k a_{q,k}$) and, $p_{q,j} = a_{q,j}/r_q^2$ is the instantaneous probability of state j in the q polarization state. Γ is defined as the diagonal matrix of inverse lifetimes with $\Gamma_{kj} = \nu_i\delta_{kj}$. W is the matrix transitions rates between different states, such as $W = \nu_i p_{q,k}$.

The particular form of W avoids matrix inversion. According to[56], defining the quasistatic propagator

$$G^s(z) = \Big(z - iL^d - i\Gamma\Big)^{-1} \tag{16}$$

which has only diagonal matrix elements, the total propagator can be written as

$$G^d(z) = G^s(z) - iG^s(z)\cdot W\cdot G^d(z). \tag{17}$$

and introducing the previous expression in (15), we get

$$I_{d,q}(\omega) = \frac{r_q^2}{\pi} Re\frac{\sum_k \frac{(a_{q,k}+ic_{q,k})/r_q^2}{\nu_i+\gamma_{q,k}+i(\omega-\omega_{q,k})}}{1-\nu_i\sum_k \frac{a_{q,k}/r_q^2}{\nu_i+\gamma_{q,k}+i(\omega-\omega_{q,k})}}. \tag{18}$$

The above expression is used to calculate the Stark-Zeeman line shape along the line of sight given by Eqs.(10), (11) and (12).

C. Electron broadening operator

The physical model of electron broadening used in PPPB is based on a semi-classical impact approximation including the effects of a strong collision term[57], and of interference[58]. It is

supposed that the emitter interacts with the plasma by binary collisions considering independent pseudo-electrons. The Debye length represents an upper cutoff beyond which the electrons do not collide. Moreover the pseudo-electrons move at constant velocities along straight trajectories. A lower cutoff is introduced to avoid the Coulomb divergence at short distances. Using the perturbation theory up to second-order in the emitter-electron interaction, the Maxwell-average operator is given by

$$\Phi(\Delta\omega) = -\frac{4\pi}{3} N_e \sqrt{\frac{2m_e}{\pi k_B T_e}} \left(\frac{\hbar}{m_e}\right)^2 \vec{R}\cdot\vec{R}\Big(C_n + G(\Delta\omega)\Big), \tag{19}$$

where $\Delta\omega$ is the frequency detuning from the line center, $\vec{R}$ is the (emitter) electron position operator operating in the subspace of principal quantum number n and C_n is the n-dependent strong collision term, with $C_2 = 1.5$, $C_3 = 1.0$, $C_4 = 0.75$, $C_5 = 0.5$ and $C_n = 0.4$ for $n > 5$.

There are many ways to estimate $G(\Delta\omega)$ (see[16] and references therein). We use the semi-classical GBK model[57]

$$G(\Delta\omega) = \frac{1}{2}\int_y^\infty \frac{e^{-x}}{x} dx \text{ with } y \approx \left(\frac{\hbar n^2}{2Z}\right)^2 \left(\frac{\Delta\omega^2 + \omega_c^2}{E_H k_B T_e}\right) \tag{20}$$

where the cutoff frequency, ω_c, linked to the upper cutoff $\rho_{max} = v_{th}/\omega_c$, given in Eq. (15) in[57]. $v_{th} = (kT/m_e)^{1/2}$ is the average thermal velocity. From the line center to ω_c the collision operator is essentially frequency independent, limiting the impact regime.

The collective properties of the electrons are usually assumed to occur through a time that corresponds to the inverse of the electron plasma frequency, $\omega_p = \sqrt{4\pi N_e e^2/m_e}$. However, if any process reduces the characteristic duration of the perturbation, the correlation can be considered lost. This is the case, for example, for high-n series lines of hydrogen, studied for plasma conditions relevant to magnetic fusion and gas discharges experiments, where the line widths are larger than the plasma frequency[59]. It is also the case, for high density ($N_e \geqslant 10^{18}\ cm^{-3}$) but relatively low temperature ($T_e \approx 1\ eV$) plasmas. Due to the large number of electrons in the Debye sphere, the correlation is lost when the electron configuration changes, i.e. when the electrons move. We use the inverse time corresponding to a configuration change $\omega_e = 2\pi/\tau_e$, where the characteristic time of the interaction is $\tau_e = r_e/v_{th}$, with the average distance $r_e = (\frac{4}{3}\ \pi N_e)^{-1/3}$. Moreover, as mentioned in the section III, it has been shown that the introduction of helical trajectories reduces the characteristic duration of the perturbation to the order of the inverse of the Larmor frequency. In this case, a cutoff at $\omega_L = eB/m_e c$ should be used[60]. Finally, for non-degenerated

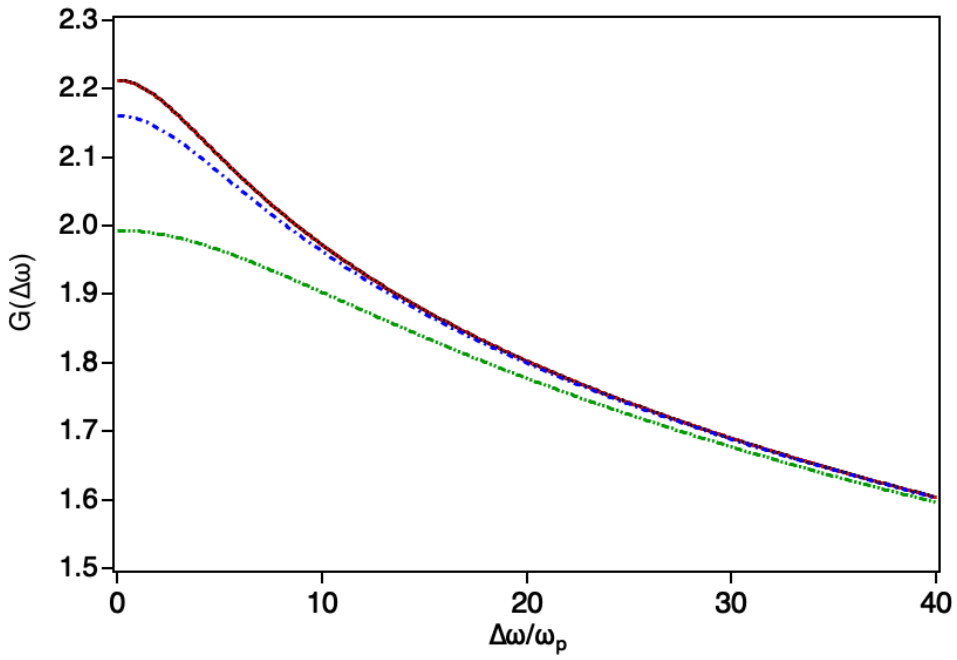

FIG. 2. $G(\Delta\omega)$ calculated for the hydrogen Lyman$-\alpha$ line at $N_e = 10^{17}\ cm^{-3}$ and $k_BT = 5\ eV$, for different different B-field values that modify the cutoff frequency ω_L: $B = 100\ tesla$ (short-dash), $B = 500\ tesla$ (dot-dash) and $B = 1\ ktesla$ (double-dot-dash). For comparison, the $G(\Delta\omega)$ functions are shown for the non-magnetized case (solid line).

systems, an additional cutoff at frequency $\omega_{\alpha\alpha'}$ between the state α and α' has been retained too[44].

Hence, the cutoff frequency ω_c, in Eq. (20) has been modified in PPPB to account for electron-electron correlations and the helical trajectories. Here, $\omega_c = max(\omega_p, \omega_e, \omega_L, \omega_{\alpha\alpha'})$.

The influence of the Larmor frequency variation on $G(\Delta\omega)$ is shown in Fig. 2, for conditions relevant to white dwarfs atmosphere (Lyman-α line at $N_e = 10^{17}\ cm^{-3}$ and $k_BT = 5\ eV$ and $B = 100,\ 500$ and$10^3\ tesla$). The $G(\Delta\omega)$ calculated for $B = 100\ tesla$ is superposed to the non-magnetized results as ω_e is larger than ω_L for those plasma conditions. For higher B-field values, the cutoff is at the Larmor frequency. As the B-field value increases, the value of $G(\Delta\omega = 0)$ decreases as well as the derivative of this function. The impact region is then extended. Such results lead to a reduction of the Stark-Zeeman line width with increasing B[40].

The impact limit, $G(\Delta\omega = 0)$, is generally used in PPPB. It has been checked that for multi-

charged ions, this approximation only affect the wing of the lines for values ω of the order of or larger than v_{th}/r_W ($r_W = \hbar n^2/Zmv_{th}$ being the Weisskopf radius).

V. SELECTED CALCULATIONS

In this section, we present different examples of applications in a broadband of plasma conditions encountered in dense gas jet discharges and laser-produced plasma experiments in which strong, controlled, static magnetic fields could be generated, as for example, by the mean of the capacitor-coil target technique[61–63]. In this technique, two parallel disks linked by a coil are irradiated by a high power nanosecond laser. Escaping hot electrons charge the target giving rise to a strongh current passing through the coil. This strong current generates sub-ns duration B-fields of strength up to one kilo-tesla.

A. Lyman$-\alpha$ lines of hydrogen-like Carbon in dense laser-produced plasmas submitted to strong external magnetic fields: a need to account for intermediate B-fields.

We investigate the Stark-Zeeman effect on the C VI Lyman-α line at 367.55 eV in a dense laser-produced plasma submitted to strong external magnetic fields experiment. For the selected plasma conditions ($N_e = 10^{19} - 10^{20}$ cm^{-3} and $T = 100$ eV), the Stark broadening is less than 0.02 eV and the fine structure of the line, that corresponds to a splitting of 0.05 eV, can be seen. Such lines are interesting because, under a magnetic field of the order of few hundred teslas, the Zeeman splitting is sufficiently strong to prevail over the Stark broadening effect and, moreover, none of the weak- or strong- field approximations are valid. The calculation of the atomic physics within intermediate B-field approximation is required.

The figures 3, 4 and 5 show the Stark-Zeeman (SZ) broadened polarized profiles for three different B-fields. They are calculated using atomic data generated within the weak-field approximation (black line) or within the intermediate-field approximation (MASCB, red line). For the sake of clarity, the π components are plotted with negative intensities. The pure Stark profiles (dot black line) are also plotted to show the modification due to the Zeeman effect on those lines. For $B = 100$ $tesla$, both approximations give quite the same Zeeman splitting and the profiles are mostly identical. For $B = 500$ $tesla$, the weak field approximation starts to be critical and

differences appear on the SZ line shapes. For $B = 10^3$ *tesla*, the Zeeman splitting being of the order of magnitude of the spin-orbit interaction, the weak-field approximation gives a drastically different B-field signature on the spectrum compared to the intermediate approximation. Using the latter, one can see a global blue-shift of the lines and different structures. In the limit of strong fields, e.g $B \sim 10^4$ *tesla*, it has been checked that the spectra calculated within the intermediate B-field approximation tend to the ones calculated within the strong field approximation, in which the spin-orbit interaction is neglected.

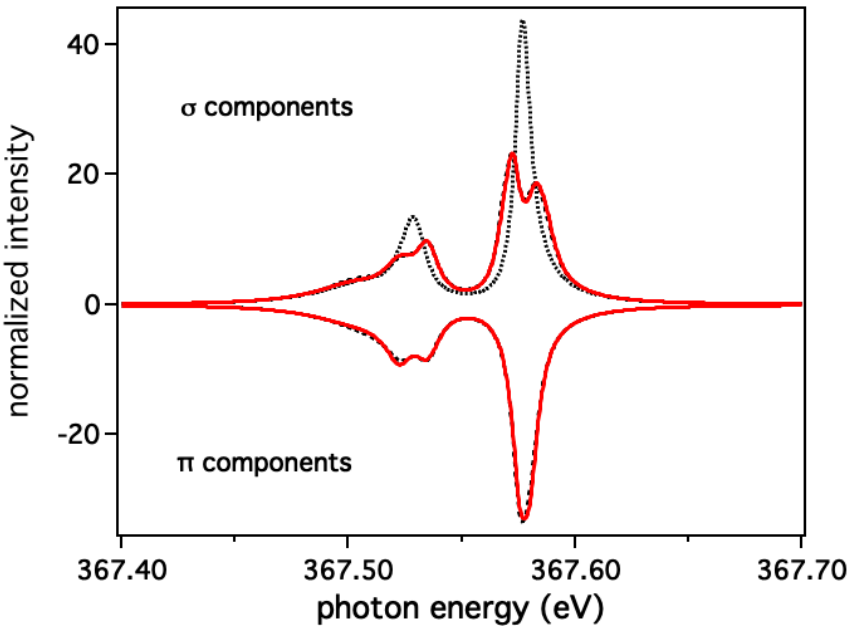

FIG. 3. Stark-Zeeman Lyman$-\alpha$ line profiles of CVI, using the weak-field approximation (dash) and the intermediate field approximation (solid) for $B = 100$ *tesla*, $N_e = 5 \times 10^{19}$ cm^{-3}, $T = 100$ eV. Short-dash line corresponds to the pure Stark profile.

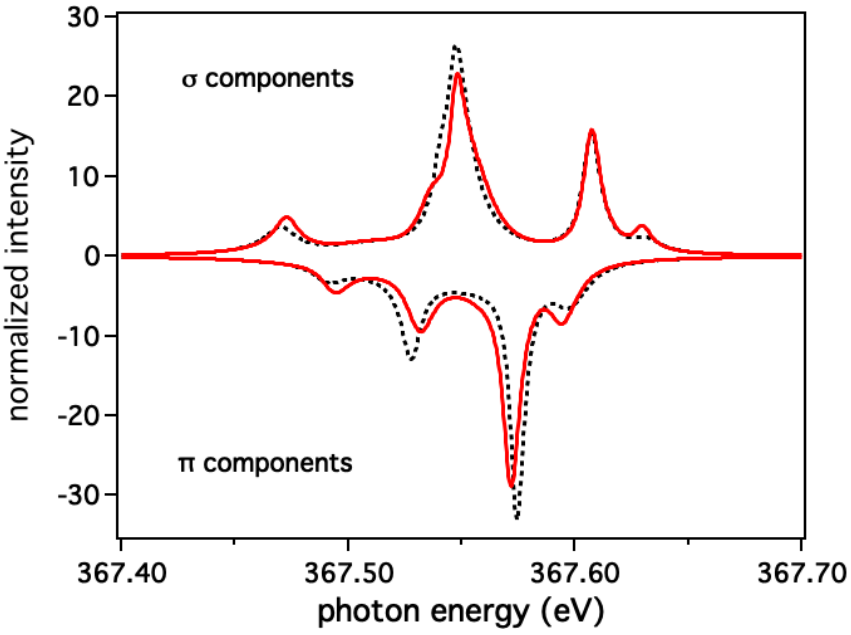

FIG. 4. The same as FIG. 3 except for $B = 500\ tesla$

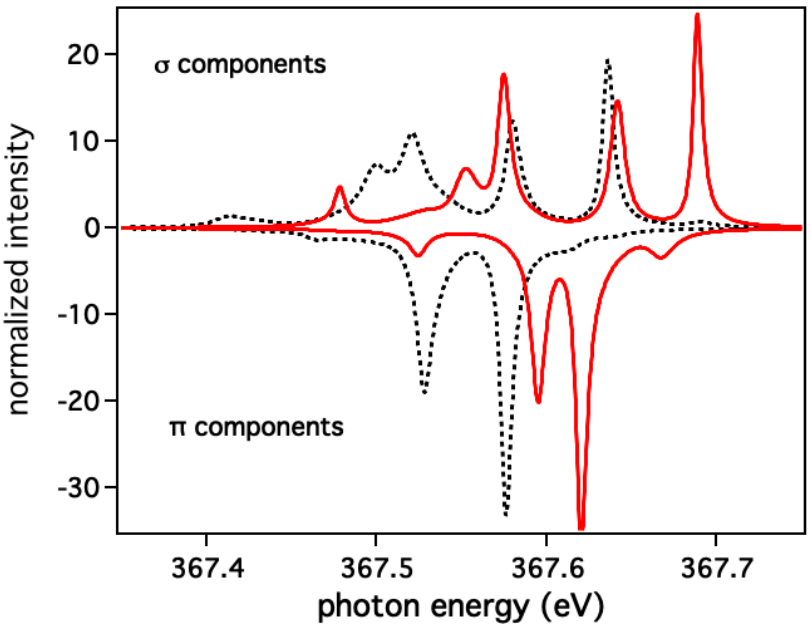

FIG. 5. The same as FIG. 3 except for $B = 10^3\ tesla$

B. Prospect on Lithium-like isoelectronic C IV, NV and O VI $n = 4 - n = 5$ lines submitted to strong external magnetic fields

Measurements of Stark broadened profiles of the $n = 4$ to $n = 5$ transitions for the Lithium-like isoelectronic sequences have been reported in[64]. They were observed in a gas-liner pinch discharge, where the plasma conditions, $10^{18} \leqslant N_e(cm^{-3}) \leqslant 2.8 \times 10^{18}$ and $8.6 \leqslant kT_e \leqslant 17\ eV$, were independently diagnosed by Thomson scattering. The spectrometer resolution was sufficiently high to well resolve the Stark broadened profiles. The width of the apparatus profile is 3%, 25% and 43% of the Stark broadened C IV, NV and O VI $n = 4 - n = 5$ transitions linewidths, respectively. Not to mention that, the width of the corresponding Doppler profiles is below 0.1% in all cases. The experimental set up described in[64] provided a benchmark for models. We have investigated the effects of strong B-fields on those lines.

Stark-Zeeman calculations are challenging here because the number of fine structure energy levels, line transitions and Stark coupling between energy levels increase with the principal quantum number. For the present calculations, levels belonging to $n = 4, 5$ and 6 have been considered. 154 fine structure energy levels associated with the upper (initial) levels and 32 fine structure energy levels associated with the lower (final) ones are then accounted for and over 1,200 electric dipole allowed transitions are taken into account in the calculations (including $\Delta n \neq 0$).

The figure 6 shows the modifications of the calculated C IV $n = 4$ to $n = 5$ line shapes under magnetic fields up to $B = 500\ tesla$, for $N_e = 2 \times 10^{18}\ cm^{-3}$ and $T_e = T_i = 10\ eV$. In both figures, the pure Stark broadened line profile, i.e. $B = 0$ calculations, are plotted together with the measured one to illustrate the very good agreement between PPP and the experimental data (taken from[64]). The Zeeman patterns of the $n = 4$ to $n = 5$ line transitions show interesting features as the line shapes corresponding to the σ components present two distinguishable peaks that split as the B-field increases, whereas the Stark-Zeeman line shapes corresponding to the π components do not really vary with B-field values.

Similar tendency is seen on the SZ line shapes of lithium-like Nitrogen and Oxygen. The figure 7 shows the Stark-Zeeman effect on the σ and π components of the C IV, NV and OVI $n = 4$ to $n = 5$ transitions.

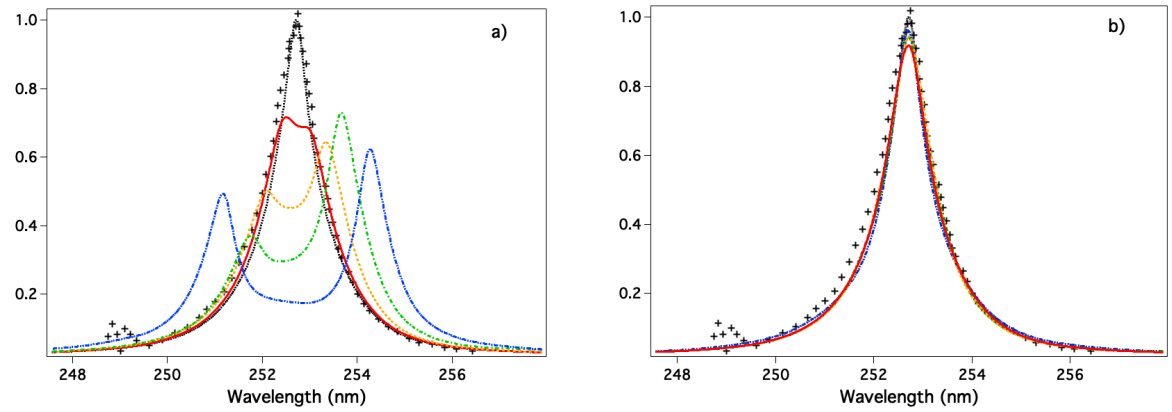

FIG. 6. Stark-Zeeman C IV $n=4$ to $n=5$ polarized line profiles for $N_e = 2\times10^{19}\ cm^{-3}$, $T = 10\ eV$, $B = 0$ (dot), $B = 100\ tesla$ (solid), $B = 200\ tesla$ (dash), $B = 300\ tesla$ (dot-dash) and $B = 500\ tesla$ (double-dot-dash). a) σ components; b) π components. The experiments[64] are plotted with solid-plus signs.

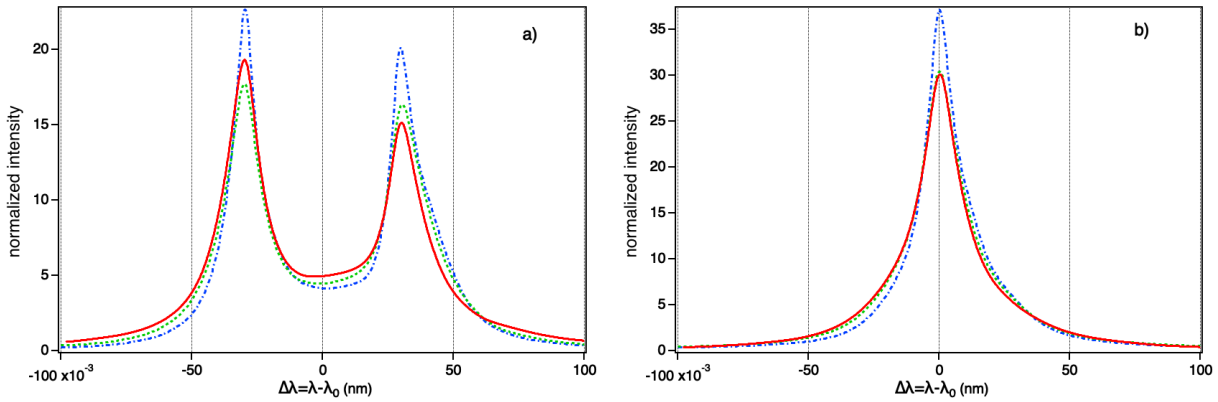

FIG. 7. Comparisons of the Stark-Zeeman broadened $n=4$ to $n=5$ line transitions for C IV (solid), N V (dash), and O VI (dot-dash) at $B = 500\ T$, $N_e = 2\times10^{18}\ cm^{-3}$, $T = 10\ eV$. a) σ components; b) π components.

By recording experimentally the $\sigma-$ and $\pi-$components simultaneously, it is possible to characterize the polarization degree of the different Stark-Zeeman emission lines

$$P(\omega) = \frac{I_\pi(\omega) - I\sigma(\omega)}{I_\pi(\omega) + I\sigma(\omega)} \tag{21}$$

The Fig. 8 shows the polarization degree calculated for the C IV $n=4$ to $n=5$ transitions for different B-field values. As the π and σ components present very different line profiles the variation of the polarization degree goes up to 70%. This case is very favorable to infer the magnetic fields because the Zeeman patterns are well observable among the Stark broadening. Neverthe-

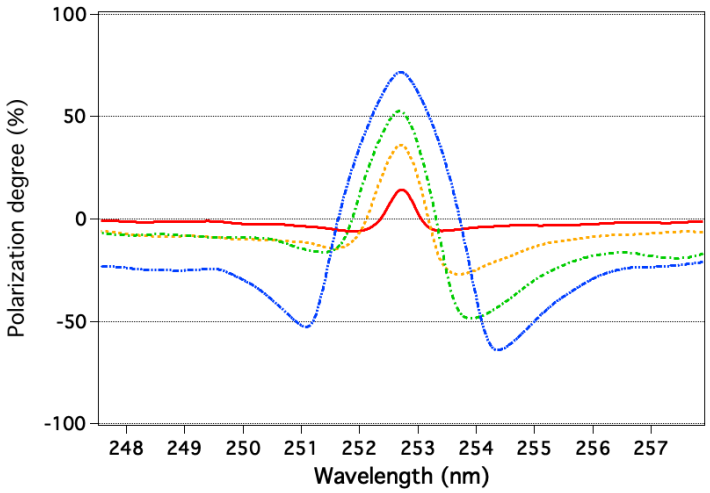

FIG. 8. Polarization degree of the C IV $n=4$ to $n=5$ lines for $N_e = 2\times10^{18}\ cm^{-3}$, $T = 10\ eV$, $B = 100\ tesla$ (solid), $B = 200\ tesla$ (dash), $B = 300\ tesla$ (dot-dash) and $B = 500\ tesla$ (double-dot-dash).

less, for cases where the Zeeman patterns tend to be masked by other broadening mechanisms, few percents of polarization degree are still experimentally measurable[65].

The Fig. 9 shows the σ and π SZ line shapes of the O VI $n = 4$ to $n = 5$ transitions calculated for a magnetic field $B = 100\ tesla$ and convolved with a Lorentzian apparatus profile with a FWHM of 0.18 nm that correspond to the detection system used in[64]. Accounting for this additional broadening, the σ components are no longer resolved and show a profile similar to the π component one. A measure of B-field from the Zeeman patterns would be unreliable, whereas it would be still feasible using the corresponding polarization degree that gives 5% at the center of the line.

The comparison of the observed and calculated polarization degree can then be in principle used as diagnostic tool to infer the magnetic field even if the Zeeman patterns are masked.

C. Ar K-shell emission in strongly magnetized plasmas

The design of a novel all-optical platform to magnetize laser-driven cylindrical implosions at the OMEGA facility and their characterization through X-ray line emission has been recently proposed[66,67]. The experimental scheme combines the laser-driven MagLIF configuration for

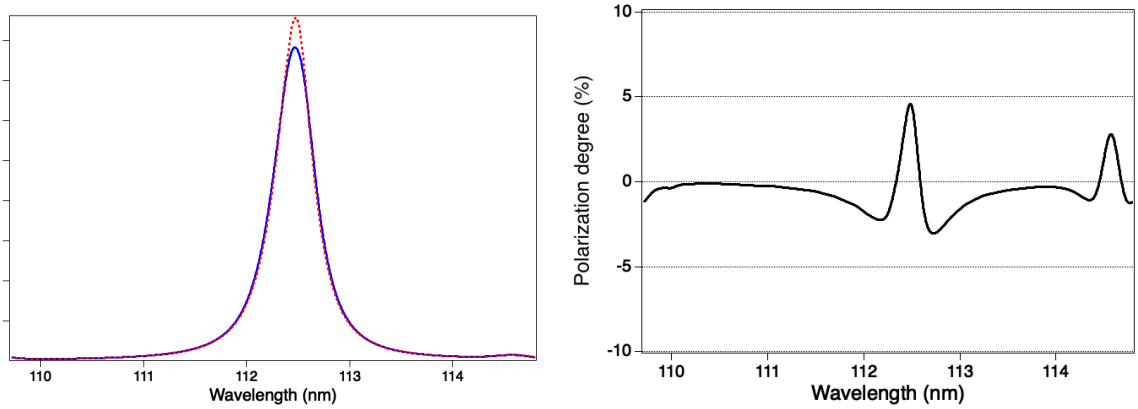

FIG. 9. Stark-Zeeman line shapes, σ (solid) and π (dash) components and the corresponding polarization degree of the O VI $n = 4$ to $n = 5$ lines for $B = 100\ tesla$ at $N_e = 2 \times 10^{18}\ cm^{-3}$ and $T = 10\ eV$.

the implosion of low-density gas filled cylindrical targets[68] with laser-driven seed B-fields[63]. A B-field exceeding 10 *ktesla* over the entire compressed core is predicted by the MHD code GORGON[69,70]. For the referred conditions, Ar K-shell spectra are expected to be observed, thanks to the high quality spectroscopic data of Ar K-shell emission lines, with spectral resolution $E/\Delta E \sim 1800$, already obtained in Inertial Fusion Confinement experiments[71,72].

Three spectral properties of dopant atoms can be exploited to infer a unique measurement of the core electron temperature and density as well as the local B-field: i) the Stark broadened line shapes which depend strongly on the electron density, ii) the relative intensity distribution of K-shell lines and associated satellites which are sensitive to the electron temperature and density[72], iii) the expected compressed B-field which is indeed strong enough to induce significant splitting, broadening and polarization effects on the K-shell emission spectra[17].

We have performed investigation on the Stark-Zeeman broadened line shapes of Ar K-shell X-ray transitions in Hydrogen- and Helium-like ions, namely Ly_α ($2p \rightarrow 1s$), Ly_β ($3p \rightarrow 1s$), Ly_γ ($4p \rightarrow 1s$) and Ly_δ ($5p \rightarrow 1s$) in H-like Ar and He_α ($1s2p \rightarrow 1s^2$), He_β ($1s3p \rightarrow 1s^2$), He_γ ($1s4p \rightarrow 1s^2$) in He-like Ar. Here a tracer amount of Ar in a deuterium plasma have been considered. A grid of plasma densities from $N_e = 3 \times 10^{22}\ cm^{-3}$ to $N_e = 3 \times 10^{24}\ cm^{-3}$ and a grid of B-field values from 10 to 80 ktesla have been retained. Since the Stark-broadened line shapes weakly depend on the electron temperature, only a representative value of 2 keV was chosen. Such detailed SZ line shapes were used in the NLTE atomic kinetics code ABAKO[73] to compute

synthetic X-ray emission spectra[17,67].

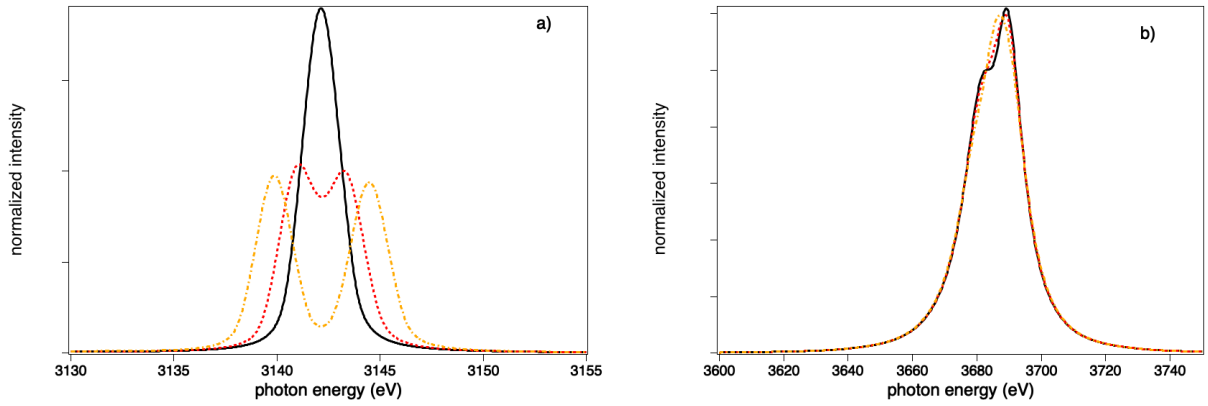

FIG. 10. Calculations of a) Ar He$-\alpha$ and b) He$-\beta$ Stark-Zeeman spectral lines for $N_e = 5 \times 10^{23}\ cm^{-3}$, $T = 2\ keV$, $B = 0$ (solid), $B = 20\ ktesla$ (dash) and $B = 40\ ktesla$ (dot-dash). A convolution with an instrumental resolution $E/\Delta E = 1800$ is performed. The observation is parallel to the magnetic field.

In the figure 10, the Stark-Zeeman lines shapes of the Ar He$-\alpha$ and He$-\beta$ calculated for two B-fields values ($B = 20\ ktesla$ and $B = 40\ ktesla$) are compared to the corresponding Stark broadened profiles ($B = 0$). The Doppler and instrumental resolution $E/\Delta E = 1800$ are accounted for. As shown in the figure, the He$-\alpha$ line are more sensitive than He$-\beta$ line in terms of Zeeman splitting. The same tendency have been seen on the Ar H-like Lyman lines. As the principal quantum number increases, the Stark broadening increases and masks the Zeeman patterns.

A possible way to measure the plasma parameters from the synthetic spectra would rely on the following: by measuring simultaneously different emission lines one could characterize plasma density and temperature from $\beta-$lines, through the Stark broadening. For the found plasma parameters, one could adjust the B-field value needed to reproduce the extra B-field-induced broadening observed in experimental $\alpha-$lines. Althought the He$-\alpha$ lines suffer from re-absorption for such plasma conditions, the latter occurs in the center of the line. As the Zeeman effect splits the lines, one can expect that the sigma components will be poorly re-absorbed, so that the B-field diagnostic will be still feasible.

VI. CONCLUSION

Atomic structure can be used for magnetized plasma characterization, as hydrogen and multi-ionized atom line emission broadens and gets polarized under strong B-fields. In this work, the main feature of the Stark-Zeeman line shape code PPPB is presented through various applications related to strongly magnetized plasmas encountered in astrophysics or in laboratory. PPPB allows calculations for a wide range of plasma conditions and it is sufficiently fast to provide line shapes to be used in radiation transport code. Zeeman effect in intermediate coupling is accounted for by the mean of the atomic physics code MASCB that generates B-field dependent atomic physics quantities. Investigation on hydrogen line series in highly magnetized astrophysical plasmas have shown that the quadratic Zeeman terms give rise to additional structures and to a global shift that increases with the principal quantum number. In high energy density plasmas, the measurement of gigagauss (10^5 *tesla*) magnetic fields using Zeeman broadened lines from highly charged ions has been proposed[74]. Investigation of quadratic term effects on the Stark-Zeeman line shapes emitted from highly charged ions may be of great importance as those lines are used as diagnostic tools. Another interesting study is the effect of helical trajectories of the charged particles produced by the presence of strong B-fields. The gyromotion of the ions and electrons may alter the dynamics of the plasma particles and thus their interaction with the plasma emitters. The present version of the code accounts for this effect by using a cutoff at the Larmor frequency in the electron broadening operator. Investigation on anisotropy and screening effects on the electronic and ionic microfield properties has to be done to improve the corresponding models in line shape codes.

ACKNOWLEDGMENTS

This work has been supported by the EUROfusion Enabling Research work programme 2017 (CfP-AWP17-IFE-CEA-02).

DATA AVAILABILITY STATEMENT

The data that support the findings of this study are available from the corresponding author upon reasonable request.

REFERENCES

[1]H. R. Griem, *Principles of plasma spectroscopy* (Principles of plasma spectroscopy. Cambridge: Cambridge U Press, 1997).

[2]H. Nguyen-Hoe, "Effet d'un champ magnetique uniforme sur les profils des raies de l'hydrogene," Journal of Quantitative Spectroscopy and Radiative Transfer **7**, 429–474 (1967).

[3]M. S. Murillo, M. E. Cox, and S. M. Carr, "Magnetized plasma microfield studies by molecular dynamics simulation," Journal of Quantitative Spectroscopy and Radiative Transfer **58**, 811–820 (1997).

[4]M. A. Gigosos and M. Á. González, "Comment on "a study of ion-dynamics and correlation effects for spectral line broadening in plasma: K-shell lines"," Journal of Quantitative Spectroscopy and Radiative Transfer **105**, 533–535 (2007).

[5]E. Stambulchik, K. Tsigutkin, and Y. Maron, "Spectroscopic method for measuring plasma magnetic fields having arbitrary distributions of direction and amplitude," Physical review letters **98**, 225001 (2007).

[6]J. Rosato, D. Reiter, V. Kotov, P. Börner, H. Capes, Y. Marandet, R. Stamm, S. Ferri, L. Godbert-Mouret, M. Koubiti, *et al.*, "Line shape modeling for radiation transport investigations in magnetic fusion plasmas," High energy density physics **5**, 93–96 (2009).

[7]G. Mathys, "The transfer of polarized light in stark broadened hydrogen lines in the presence of a magnetic field," Journal of Quantitative Spectroscopy and Radiative Transfer **44**, 143–151 (1990).

[8]A. Derevianko and E. Oks, "Generalized theory of ion impact broadening in magnetized plasmas and its applications for tokamaks," Physical review letters **73**, 2059 (1994).

[9]S. Brillant, G. Mathys, and C. Stehle, "Hydrogen line formation in dense magnetized plasmas," Astronomy and Astrophysics **339**, 286–297 (1998).

[10]S. Günter and A. Könies, "Diagnostics of dense plasmas from the profile of hydrogen spectral lines in the presence of a magnetic field," Journal of Quantitative Spectroscopy and Radiative Transfer **62**, 425–431 (1999).

[11]L. Godbert-Mouret, M. Koubiti, R. Stamm, K. Touati, B. Felts, H. Capes, Y. Corre, R. Guirlet, and C. De Michelis, "Spectroscopy of magnetized plasmas," Journal of Quantitative Spectroscopy and Radiative Transfer **71**, 365–372 (2001).

[12]M. Adams, R. Lee, H. Scott, H. Chung, and L. Klein, "Complex atomic spectral line shapes in the presence of an external magnetic field," Physical Review E **66**, 066413 (2002).

[13]X.-d. Li, S.-s. Han, C. Wang, and Z.-z. Xu, "Ultrahigh magnetic field diagnostic with spectral profile calculation," Journal of Quantitative Spectroscopy and Radiative Transfer **76**, 31–43 (2003).

[14]S. Ferri, A. Calisti, C. Mossé, L. Mouret, B. Talin, M. A. Gigosos, M. A. González, and V. Lisitsa, "Frequency-fluctuation model applied to stark-zeeman spectral line shapes in plasmas," Physical Review E **84**, 026407 (2011).

[15]C. A. Iglesias, "Efficient algorithms for stark–zeeman spectral line shape calculations," High Energy Density Physics **9**, 737–744 (2013).

[16]F. Gilleron and J.-C. Pain, "Zest: A fast code for simulating zeeman-stark line-shape functions," Atoms **6**, 11 (2018).

[17]J. J. Santos, M. Bailly-Grandvaux, M. Ehret, A. Arefiev, D. Batani, F. Beg, A. Calisti, S. Ferri, R. Florido, P. Forestier-Colleoni, *et al.*, "Laser-driven strong magnetostatic fields with applications to charged beam transport and magnetized high energy-density physics," Physics of Plasmas **25**, 056705 (2018).

[18]C. Liu, K. Matsuo, S. Ferri, H.-K. Chung, S. Lee, S. Sakata, K. F. F. Law, H. Morita, B. Pollock, J. Moody, *et al.*, "Design of zeeman spectroscopy experiment with magnetized silicon plasma generated in the laboratory," High Energy Density Physics **33**, 100710 (2019).

[19]R. D. Cowan, *The theory of atomic structure and spectra*, 3 (Univ of California Press, 1981).

[20]I. Grant, B. McKenzie, P. Norrington, D. Mayers, and N. Pyper, "An atomic multiconfigurational dirac-fock package," Computer Physics Communications **21**, 207–231 (1980).

[21]M. F. Gu, "The flexible atomic code," Canadian Journal of Physics **86**, 675–689 (2008).

[22]E. Stambulchik, "cFAC code in GitHub kernel description,".

[23]B. Cagnac and J. C. P. Peyroula, *Physique atomique, tome 2: applications de la mecanique quantique* (Bordas, 1982).

[24]J. C. Slater, "Quantum theory of atomic structure," Tech. Rep. (1960).

[25]M. Litsarev and O. Ivanov, "Multiconfiguration hartree-fock method: Direct diagonalization for the construction of a multielectron basis," Journal of Experimental and Theoretical Physics **111**, 22–26 (2010).

[26]E. Hill, "Calculation of unit tensor operators using a restricted set of slater determinants," Journal of Quantitative Spectroscopy and Radiative Transfer **140**, 1–6 (2014).

[27]E. U. Condon, E. Condon, and G. Shortley, *The theory of atomic spectra* (Cambridge University Press, 1935).

[28]J. D. Talman and W. F. Shadwick, "Optimized effective atomic central potential," Physical Review A **14**, 36 (1976).

[29]J. Krieger, Y. Li, and G. Iafrate, "Systematic approximations to the optimized effective potential: Application to orbital-density-functional theory," Physical Review A **46**, 5453 (1992).

[30]R. Garstang and S. Kemic, "Hydrogen and helium spectra in large magnetic fields," Astrophysics and Space Science **31**, 103–115 (1974).

[31]S. O. Kepler, I. Pelisoli, S. Jordan, S. J. Kleinman, D. Koester, B. Külebi, V. Peçanha, B. G. Castanheira, A. Nitta, J. E. d. S. Costa, *et al.*, "Magnetic white dwarf stars in the sloan digital sky survey," Monthly Notices of the Royal Astronomical Society **429**, 2934–2944 (2013).

[32]J. Rosato, "Hydrogen line shapes in plasmas with large magnetic fields," Atoms **8**, 74 (2020).

[33]A. Raji, J. Rosato, R. Stamm, and Y. Marandet, "New analysis of balmer line shapes in magnetic white dwarf atmospheres," The European Physical Journal D **75**, 1–4 (2021).

[34]D. R. Inglis and E. Teller, "Ionic depression of series limits in one-electron spectra." The Astrophysical Journal **90**, 439 (1939).

[35]T. Ott and M. Bonitz, "Diffusion in a strongly coupled magnetized plasma," Physical review letters **107**, 135003 (2011).

[36]S. D. Baalrud and J. Daligault, "Transport regimes spanning magnetization-coupling phase space," Physical Review E **96**, 043202 (2017).

[37]D. J. Bernstein, T. Lafleur, J. Daligault, and S. D. Baalrud, "Friction force in strongly magnetized plasmas," Physical Review E **102**, 041201 (2020).

[38]E. Oks, "Influence of magnetic-field-caused modifications of trajectories of plasma electrons on spectral line shapes: Applications to magnetic fusion and white dwarfs," Journal of Quantitative Spectroscopy and Radiative Transfer **171**, 15–27 (2016).

[39]J. Rosato, S. Ferri, and R. Stamm, "Influence of helical trajectories of perturbers on stark line shapes in magnetized plasmas," Atoms **6**, 12 (2018).

[40]S. Alexiou, "Line shapes in a magnetic field: Trajectory modifications i: Electrons," Atoms **7**, 52 (2019).

[41]S. Alexiou, "Line shapes in a magnetic field: Trajectory modifictions ii: Full collision-time statistics," Atoms **7**, 94 (2019).

[42]C. Deutsch, "Electric microfield distributions in plasmas in presence of a magnetic field," Physics Letters A **30**, 381–382 (1969).

[43]S. Ferri, "Study of plasma microfield properties in highly magnetized plasmas," (2018) unpublished results.

[44]A. Calisti, F. Khelfaoui, R. Stamm, B. Talin, and R. Lee, "Model for the line shapes of complex ions in hot and dense plasmas," Physical Review A **42**, 5433 (1990).

[45]A. Calisti, L. Godbert, R. Stamm, and B. Talin, "Fast numerical methods for line shape studies in hot and dense plasmas," Journal of Quantitative Spectroscopy and Radiative Transfer **51**, 59–64 (1994).

[46]N. Woolsey, A. Asfaw, B. Hammel, C. Keane, C. Back, A. Calisti, C. Mosse, R. Stamm, B. Talin, J. Wark, *et al.*, "Spectroscopy of compressed high energy density matter," Physical Review E **53**, 6396 (1996).

[47]N. Woolsey, B. Hammel, C. Keane, A. Asfaw, C. Back, J. Moreno, J. Nash, A. Calisti, C. Mosse, R. Stamm, *et al.*, "Evolution of electron temperature and electron density in indirectly driven spherical implosions," Physical Review E **56**, 2314 (1997).

[48]B. Talin, A. Calisti, L. Godbert, R. Stamm, R. Lee, and L. Klein, "Frequency-fluctuation model for line-shape calculations in plasma spectroscopy," Physical Review A **51**, 1918 (1995).

[49]M. Abramowitz and I. Stegun, "Handbook of mathematical functions. original work published 1964," (1972).

[50]B. Talin, E. Dufour, A. Calisti, M. A. Gigosos, M. A. Gonzalez, T. del Rio Gaztelurrutia, and J. W. Dufty, "Molecular dynamics simulation for modelling plasma spectroscopy," Journal of Physics A: Mathematical and General **36**, 6049 (2003).

[51]C. A. Iglesias, H. E. DeWitt, J. L. Lebowitz, D. MacGowan, and W. B. Hubbard, "Low-frequency electric microfield distributions in plasmas," Physical Review A **31**, 1698 (1985).

[52]C. Iglesias, F. Rogers, R. Shepherd, A. Bar-Shalom, M. Murillo, D. Kilcrease, A. Calisti, and R. Lee, "Fast electric microfield distribution calculations in extreme matter conditions," Journal of Quantitative Spectroscopy and Radiative Transfer **65**, 303–315 (2000).

[53]C. Hooper Jr, "Low-frequency component electric microfield distributions in plasmas," Physical Review **165**, 215 (1968).

[54]N. Woolsey, B. Hammel, C. Keane, C. Back, J. Moreno, J. Nash, A. Calisti, C. Mosse, L. Godbert, R. Stamm, *et al.*, "Spectroscopic line shape measurements at high densities," Journal of Quantitative Spectroscopy and Radiative Transfer **58**, 975–989 (1997).

[55]S. Ferri, A. Calisti, C. Mossé, J. Rosato, B. Talin, S. Alexiou, M. A. Gigosos, M. A. González, D. González-Herrero, N. Lara, *et al.*, "Ion dynamics effect on stark-broadened line shapes: A cross-comparison of various models," Atoms **2**, 299–318 (2014).

[56]A. Calisti, C. Mossé, S. Ferri, B. Talin, F. Rosmej, L. Bureyeva, and V. Lisitsa, "Dynamic stark broadening as the dicke narrowing effect," Physical Review E **81**, 016406 (2010).

[57]H. R. Griem, M. Blaha, and P. C. Kepple, "Stark-profile calculations for lyman-series lines of one-electron ions in dense plasmas," Physical Review A **19**, 2421 (1979).

[58]E. Galtier, F. Rosmej, A. Calisti, B. Talin, C. Mossé, S. Ferri, and V. Lisitsa, "Interference effects and stark broadening in xuv intrashell transitions in aluminum under conditions of intense xuv free-electron-laser irradiation," Physical Review A **87**, 033424 (2013).

[59]S. Ferri, A. Calisti, R. Stamm, B. Talin, R. Lee, and L. Klein, "Electronic broadening model for high-n balmer line profiles," Physical Review E **58**, R6943 (1998).

[60]E. Maschke and D. Voslamber, "Stark broadening of hydrogen lines in strong magnetic fields," in *Phenomena in Ionized Gases, Volume II, VII International Conference* (1966) p. 568.

[61]H. Daido, F. Miki, K. Mima, M. Fujita, K. Sawai, H. Fujita, Y. Kitagawa, S. Nakai, and C. Yamanaka, "Generation of a strong magnetic field by an intense co 2 laser pulse," Physical review letters **56**, 846 (1986).

[62]S. Fujioka, Z. Zhang, K. Ishihara, K. Shigemori, Y. Hironaka, T. Johzaki, A. Sunahara, N. Yamamoto, H. Nakashima, T. Watanabe, *et al.*, "Kilotesla magnetic field due to a capacitor-coil target driven by high power laser," Scientific reports **3**, 1–7 (2013).

[63]J. Santos, M. Bailly-Grandvaux, L. Giuffrida, P. Forestier-Colleoni, S. Fujioka, Z. Zhang, P. Korneev, R. Bouillaud, S. Dorard, D. Batani, *et al.*, "Laser-driven platform for generation and characterization of strong quasi-static magnetic fields," New Journal of Physics **17**, 083051 (2015).

[64]S. Glenzer, T. Wrubel, S. Buscher, H.-J. Kunze, L. Godbert, A. Calisti, R. Stamm, B. Talin, J. Nash, R. Lee, *et al.*, "Spectral line profiles of n= 4 to n= 5 transitions in c iv, nv and o vi," Journal of Physics B: Atomic, Molecular and Optical Physics **27**, 5507 (1994).

[65]T. Fujimoto and A. Iwamae, *Plasma polarization spectroscopy*, Vol. 44 (Springer, 2008).

[66]M. Bailly-Grandvaux, S. McGuffey, F. Beg, S. Ferri, A. Calisti, J. Davies, R. Florido, M. Gigosos, J. Honrubia, R. Mancini, *et al.*, "An all-optical platform to characterize strongly magnetized hot dense plasmas at> 10 kt," in *APS Division of Plasma Physics Meeting Abstracts*, Vol. 2020 (2020) pp. BO07–005.

[67]R. Florido, C. Walsh, M. Bailly-Grandvaux, F. Beg, C. McGuffey, A. Calisti, S. Ferri, M. Gigosos, R. Mancini, T. Nagayama, *et al.*, "Spectroscopic and mhd modeling of magnetized cylindrical implosions using a laser-produced seed b-field," in *APS Division of Plasma Physics Meeting Abstracts*, Vol. 2020 (2020) p. GP17.00009.

[68]J. Davies, D. Barnak, R. Betti, E. Campbell, V. Y. Glebov, E. Hansen, J. Knauer, J. Peebles, and A. Sefkow, "Inferring fuel areal density from secondary neutron yields in laser-driven magnetized liner inertial fusion," Physics of Plasmas **26**, 022706 (2019).

[69]C. Walsh, K. McGlinchey, J. Tong, B. Appelbe, A. Crilly, M. Zhang, and J. Chittenden, "Perturbation modifications by pre-magnetisation of inertial confinement fusion implosions," Physics of Plasmas **26**, 022701 (2019).

[70]C. Walsh, J. Chittenden, D. Hill, and C. Ridgers, "Extended-magnetohydrodynamics in underdense plasmas," Physics of Plasmas **27**, 022103 (2020).

[71]N. Woolsey, B. Hammel, C. Keane, C. Back, J. Moreno, J. Nash, A. Calisti, C. Mosse, R. Stamm, B. Talin, *et al.*, "Competing effects of collisional ionization and radiative cooling in inertially confined plasmas," Physical Review E **57**, 4650 (1998).

[72]H.-K. Chung and R. Lee, "Applications of nlte population kinetics," High Energy Density Physics **5**, 1–14 (2009).

[73]R. Florido, R. Rodríguez, J. Gil, J. Rubiano, P. Martel, E. Mínguez, and R. Mancini, "Modeling of population kinetics of plasmas that are not in local thermodynamic equilibrium, using a versatile collisional-radiative model based on analytical rates," Physical Review E **80**, 056402 (2009).

[74]J. F. Seely, "Gigagauss magnetic field measurements using zeeman broadening of ne-like transitions in highly charged ions," Review of Scientific Instruments **92**, 053535 (2021).